Robust features of a turbulent boundary layer subjected to high-intensity free-stream turbulence

R. Jason Hearst[1,3]†, Eda Dogan[2,3] and Bharathram Ganapathisubramani[3]

[1]Department of Energy and Process Engineering, Norwegian University of Science and Technology, Trondheim, NO-7491, Norway

[2]Linné FLOW Centre, KTH Mechanics, Stockholm, SE-10044, Sweden

[3]Engineering and the Environment, University of Southampton, Southampton, SO17 1BJ, United Kingdom

(Received xx; revised xx; accepted xx)

The influence of the large scale organisation of free-stream turbulence on a turbulent boundary layer is investigated experimentally in a wind tunnel through hot-wire measurements. An active grid is used to generate high-intensity free-stream turbulence with $7.2\% \leqslant u'_\infty/U_\infty \leqslant 13.0\%$ and $302 \leqslant Re_{\lambda,\infty} \leqslant 760$. In particular, several cases are produced with fixed u'_∞/U_∞ and $Re_{\lambda,\infty}$, but up to a 65% change in $L_{u,\infty}/\delta$. It is shown that while qualitatively the spectra at various wall-normal positions in the boundary layer look similar, there are quantifiable differences at the large wavelengths all the way to the wall. Nonetheless, profiles of the longitudinal statistics up to fourth-order are well collapsed between cases at the same u'_∞/U_∞. It is argued that a larger separation of the integral scale would not yield a different result, nor would it be physically realisable. Comparing cases across the wide range of turbulence intensities and free-stream Reynolds numbers tested, it is demonstrated that the near-wall spectral peak is independent of the free-stream turbulence, and seemingly universal. The outer peak was also found to be described by a set of global scaling laws, and hence both the near-wall and outer spectral peaks can be predicted *a priori* with only knowledge of the free-stream spectrum, δ, and U_τ. Finally, a conceptual model is suggested that attributes the increase in U_τ as u'_∞/U_∞ increases to the build-up of energy at large wavelengths near the wall because that energy cannot be transferred to the universal near-wall spectral peak.

Key words: (to be entered by typesetter)

1. Introduction

A canonical zero-pressure-gradient turbulent boundary layer offers several mathematical simplifications that make it a desirable flow for experimental research, however, it is not without limitations. For instance, very large facilities are required to produce Reynolds numbers, $Re_\tau = U_\tau\delta/\nu$ where U_τ is the friction velocity and δ is the boundary layer thickness, that begin to approach those in flows of practical interest (c.f., Nickels *et al.* (2005, 2007), Klewicki (2010), Vincenti *et al.* (2013)). Alternatively, a boundary

† Email address for correspondence: jason.hearst@ntnu.no

layer subjected to free-stream turbulence (FST) can be studied to gain significant insight on the mechanics of wall-bounded flows (Dogan *et al.* 2017). For instance, free-stream turbulence intensity (u'_∞/U_∞) is a dominant factor in promoting laminar-to-turbulent transition of a developing boundary layer, influencing both the start of the transition region and its length (Fransson *et al.* 2005). With direct numerical simulations (DNS), it has been demonstrated that FST also influences streak instabilities (Hack & Zaki 2014) and turbulent spots in bypass transition (Kreilos *et al.* 2016; Wu *et al.* 2017). Furthermore, the DNS of Brandt *et al.* (2004) showed that if $u'_\infty/U_\infty = 4.7\%$ was fixed, then transition occurred earlier for larger values of the integral length scale in the free-stream (L_∞). Shahinfar & Fransson (2011) later performed a series of wind tunnel experiments and confirmed this result for low u'_∞/U_∞, but noted that the opposite appeared to be true for higher u'_∞/U_∞. Thus, it would appear that both u'_∞/U_∞ and L_∞ are parameters to which a boundary layer is sensitive if subjected to free-stream turbulence.

There has also been a focus on the mechanisms and interactions of FST and a TBL once the flow has fully transitioned to turbulence. Castro (1984) showed that the skin friction increased with u'_∞/U_∞ for low $Re_\theta = U_\infty\theta/\nu$, where $\theta = \int_0^\infty (u(y)/U_\infty)(1-u(y)/U_\infty)\,\mathrm{d}y$ is the boundary layer momentum thickness. In a pair of studies, Hancock & Bradshaw (1983, 1989) also probed the relative impact of the free-stream turbulence intensity and length scale on the boundary layer. Their set-up consisted of a flat plate placed in grid-turbulence flows. They changed their external length scale and turbulence intensity by moving the plate's leading edge relative to the grid position and performing scans at different locations. This gave them a parameter space roughly spanning $2\% \leqslant u'_\infty/U_\infty \leqslant 6\%$ and $0.7 \leqslant L^u_e/\delta_{995} \leqslant 4.9$, where they defined their length scale as a dissipation length scale in the free-stream assuming isotropy and δ was estimated based on where the local velocity reached 99.5% of the free-stream velocity. They suggested the skin friction scaled with a joint parameter of the turbulence intensity and free-stream scale they defined as $\beta = (u'_\infty/U_\infty)/\left(L^u_e/\delta_{995} + 2\right)$. This experiment was undoubtedly insightful, but not without limitations. For instance, the achievable u'_∞/U_∞ at the time was low because only static grids were in common usage for producing approximately homogeneous free-stream turbulence. Because of this, the authors were required to vary their measurement station in the range $12 \leqslant x/M \leqslant 59$ to achieve their desired parameter space. This significantly changes the time the boundary layer and free-stream turbulence have evolved in each other presence. Furthermore, some of these measurements (particularly at their highest u'_∞/U_∞ and L^u_e/δ_{995}) were performed for $x/M < 20$ where some residual inhomogeneities remain in the free-stream and the Reynolds shear stress components are not guaranteed to have reached their far-field states (Corrsin 1963; Ertunç *et al.* 2010; Isaza *et al.* 2014; Hearst & Lavoie 2016). Moreover, the underlying assumptions used to estimate a meaningful dissipation length scale in the manner employed by Hancock & Bradshaw (1983, 1989) are not yet valid in this region because the balance between dissipation and the large scale energy is still evolving (Valente & Vassilicos 2012; Hearst & Lavoie 2014; Vassilicos 2015). There is thus a need to investigate these flows further without these limitations.

To expand the range of realisable turbulence intensities (up to $u'_\infty/U_\infty \sim 10\%$), Sharp *et al.* (2009) used a similar set-up to the pioneering works, but generated their FST with an active grid based on the design of Makita (1991). They similarly found that FST influenced the wall shear stress but also noted that the spectrogram composed of the pre-multiplied spectra at various wall-normal positions produced the distinctive inner and outer spectral peak geometry reminiscent of canonical high Re_τ TBLs as described by Hutchins & Marusic (2007*a*). Dogan *et al.* (2016) explored this further and clearly

identified the near-wall spectral peak as being located in the same position as for a canonical TBL by using a smaller probe that allowed them to approach the wall. They also identified that a log-region existed whose fitting parameters roughly matched those found by Marusic *et al.* (2013) for high Re_τ canonical wall-bounded flows; the log-law is given by,

$$U^+ = \frac{1}{\kappa}\ln\left(y^+\right) + \mathcal{B}, \tag{1.1}$$

where U is the local mean velocity, y is the wall-normal position, κ and $\mathcal{B}$ are fitting parameters, and the superscript $\cdot^+$ indicates normalisation by inner (wall) units, i.e., $U^+ = U/U_\tau$ and $y^+ = yU_\tau/\nu$. Significantly, Dogan *et al.* (2016, 2017) also showed that the scale interactions, as assessed through the amplitude modulation mechanisms established by Hutchins & Marusic (2007*b*), were preserved when FST was used to increase Re_τ. The implication of this is that it may be possible to use FST in a traditional wind tunnel to study TBLs at higher Re_τ than achievable without FST and without the need of a large facility.

Despite continued research in this area with both direct implications for practical flows and that offers insight into high Re_τ boundary layers at a traditional laboratory scale, there has been no investigation on the effect of integral length scale for constant turbulence intensity at a fixed far-field position, and at high turbulence intensities. The significance of using a fixed downstream position is that the evolution to that point is thus comparable between cases, and should be chosen to be sufficiently far from the grid such that the free-stream flow field has reached some canonical state of decaying turbulence; Corrsin (1963) suggested $x/M > 30$. The present study thus focusses on investigating multiple cases with fixed turbulence intensities and Reynolds numbers, but varying large scale organisation. Moreover, higher turbulence intensities and Reynolds numbers than previous works are achieved by using an active grid to generate the FST. This not only provides new insights on the effects of FST on TBL but also allows us to test the hypothesis of Marusic *et al.* (2017) that the increase of near-wall peak turbulence intensity with increasing Re_τ is *only* due to the superposition of outer coherent motions. Here, we will be able to impose a wide range of outer motions (different strengths and intensity) that can penetrate down to the wall and alter near-wall turbulence.

2. Experimental procedure & free-stream characteristics

The experimental database used in the present study is a combination of the data acquired by Dogan *et al.* (2016, 2017), supplemented with some new test-cases. The experimental apparatus and acquisition protocol used for the new cases is the same as described by Dogan *et al.* (2017). In short, a rake of four single-wire hot-wires was traversed through a TBL subjected to FST in the 0.9 m $\times$ 0.6 m $\times$4.5 m suction wind tunnel at the University of Southampton. The TBL was formed over a false-floor/boundary layer plate placed in the wind tunnel and was passively tripped. The FST was generated with an active grid placed at the inlet of the test-section. Measurements were performed at a fixed position $43M$ downstream of the grid and $Re_\theta > 2000$ for all measurements making the influence of the tripping mechanism negligible (Schlatter & Örlü 2012). The set-up of Dogan *et al.* (2016) was similar to the above, except only a single wire was traversed through the TBL with another fixed in the free-stream. See Dogan *et al.* (2016, 2017) for more details on the experimental set-ups.

The test-cases used in the present study are summarized in table 1. They are labelled with letters in order of increasing u'_∞/U_∞. Additionally, they are separated into groups where free-stream turbulence intensity (u'_∞/U_∞) and the Taylor microscale Reynolds

number ($Re_{\lambda,\infty} = u'_\infty \lambda_\infty / \nu$) are approximately matched; the Taylor microscale was estimated assuming local isotropy in the free-stream,

$$\lambda^2 = \frac{\langle u^2 \rangle}{\langle (\partial u/\partial x)^2 \rangle}. \tag{2.1}$$

Streamwise velocity gradients were approximated with Taylor's frozen flow hypothesis ($\partial(\cdot)/\partial t = U \partial(\cdot)/\partial x$) and a sixth-order centred-difference scheme; the latter has been shown to balance the needs of spatio-temporal resolution and high-frequency noise (Hearst *et al.* 2012). In table 1, the integral length scale was estimated from,

$$L_u = \int_0^{r_0} \frac{\langle u(x)u(x+r) \rangle}{\langle u^2 \rangle} \, \mathrm{d}r, \tag{2.2}$$

where r_0 is the first zero-crossing of the autocorrelation. The boundary layer parameters listed in the table (δ, U_τ, κ) were fit using the approach of Rodríguez-López *et al.* (2015) as modified for FST by Esteban *et al.* (2017). Due to the relatively high Re_τ of the present experiments and the $\ell = 1$ mm sensing length of the hot-wire probes, the inner-unit length of the probes ranged $18 \leqslant \ell^+ \leqslant 33$. As such, the variance in the near-wall region was compensated for using the approach of Smits *et al.* (2011). Any differences between the values reported in table 1 and our earlier works are a result of the different fitting process used here and the adjustments for spatial resolution.

The incoming conditions for the various test-cases were changed by adjusting the active grid settings as well as the incoming Reynolds number. The grid was operated in one of two modes: 'synchronous' or 'fully random'. In 'synchronous' mode, all motors of the grid were updated simultaneously at 1 Hz. In 'fully random' mode, updates to each motor of the grid were randomised at intervals between 0.4 and 20 Hz. The actuation velocity of the wings (Ω) was varied to produce different free-stream conditions. The range of Ω is shown for each case in table 1 and was always a top-hat distribution. The chosen test cases were modelled after those of Kang *et al.* (2003), Larssen & Devenport (2011), and Hearst *et al.* (2016). Additionally, two different wing geometries were used: solid square wings or wings with holes. Changing the wing geometry has been shown to offset the produced u'_∞/U_∞ (Thormann & Meneveau 2014; Hearst & Lavoie 2015; Dogan *et al.* 2016).

The free-stream velocity spectra are shown for all cases in figure 1. In figure 1(a), the spectra are normalised by λ which is expected to collapse the spectra in the scaling (or inertial) range as shown. The slope of the nearly two decade long scaling range is close to, but not exactly, $k_x^{-5/3}$; this agrees with previous active grid studies (Mydlarski & Warhaft 1996; Hearst & Lavoie 2015). The same spectra are shown in pre-multiplied form plotted against δ-normalised wavelength ($\zeta_x = 2\pi/k_x$) in figure 1(b). As also shown by Dogan *et al.* (2016), the peak in the pre-multiplied spectra for all cases is roughly collapsed around $\zeta_x = 10\delta$. Figure 1 highlights two key features of the flow for all cases. First, and not insignificantly, these are relatively high-$Re_{\lambda,\infty}$ FST flows and as such their spectral shape does not significantly vary between cases. This is not a consequence of poor choice of test cases, but rather is a consequence of the governing fluid dynamics that results in a spectrum that may be approximately described by the Richardson-Kolmogorov cascade and cannot be significantly changed. Second, at this evolution distance ($x/M = 43$) downstream of the turbulence generation the spectra appear to have all taken-on a rough form where their pre-multiplied peak is approximately 10δ. Given that δ, u'_∞/U_∞ and Re_τ change by factors of 0.5, 2, and 3, respectively, across all cases in table 1, figure 1(b) is highly suggestive that the boundary layer adjusts such that the peak in the pre-multiplied turbulence is at $\sim 10\delta$ and that this not simply a coincidence.

Case	Ω [Hz]	Wings	U_∞ [m/s]	u'_∞/U_∞ [%]	$Re_{\lambda,\infty}$	$L_{u,\infty}$ [m]	δ [m]	U_τ [m/s]	Re_τ	Re_θ	κ	Symbol
A	4	Holes	6.1	7.2	302	0.27	0.11	0.27	1890	2940	0.40	◇
B	5.25 ± 1.75	Holes	6.2	7.3	322	0.27	0.11	0.27	1960	2760	0.38	▷
C	4 ± 2	Holes	6.1	7.4	319	0.23	0.11	0.27	1960	2770	0.37	∗
D	4	Holes	8.1	7.7	390	0.33	0.11	0.35	2480	3860	0.39	▽
E	4 ± 2	Holes	8.1	7.8	412	0.28	0.11	0.35	2420	3730	0.39	★
F	5.25 ± 1.75	Holes	8.2	7.9	417	0.29	0.11	0.35	2520	3830	0.39	◁
G†	4 ± 2	Holes	9.9	8.1	460	0.33	0.13	0.43	3590	4550	0.41	○
H†‡	2 ± 1	Holes	8.9	8.2	446	0.22	0.13	0.38	3200	4030	0.40	□
I	5.25 ± 1.75	Holes	12.2	8.5	607	0.39	0.14	0.51	4550	5870	0.39	△
J	4 ± 2	Holes	12.2	8.6	609	0.36	0.14	0.51	4490	5980	0.39	★
K	4	Solid	8.0	11.9	515	0.42	0.17	0.35	3900	4990	0.42	■
L	5.25 ± 1.75	Solid	8.1	12.1	533	0.36	0.17	0.35	3960	5340	0.41	▼
M	4 ± 2	Solid	8.0	12.1	532	0.35	0.16	0.35	3760	4430	0.41	♦
N†	4 ± 2	Solid	10.0	12.2	620	0.26	0.16	0.44	4480	5000	0.44	▶
O	4	Solid	9.8	12.4	607	0.43	0.16	0.43	4510	4400	0.43	◀
P	5.25 ± 1.75	Solid	11.6	13.0	750	0.44	0.17	0.49	5360	7530	0.42	●
Q	4 ± 2	Solid	11.7	13.0	760	0.42	0.16	0.49	5240	7620	0.44	▲

TABLE 1. Flow parameters for all test-cases. The dagger (†) identifies test-cases acquired with the set-up of Dogan *et al.* (2017); all other test-cases are from Dogan *et al.* (2016). The double-dagger (‡) indicates the test performed in 'fully random' mode; all other tests were conducted in 'synchronous' mode.

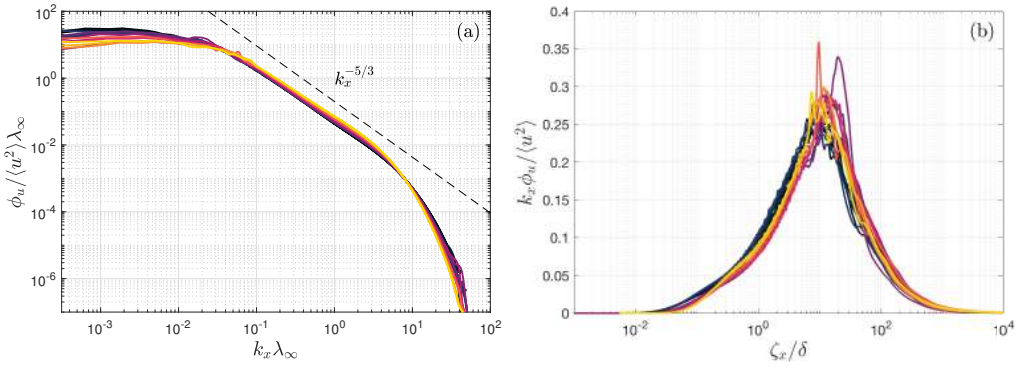

FIGURE 1. Velocity spectra in the free-stream (a) normalized by Taylor scales and (b) in pre-multiplied form. Lightest to darkest lines represent increasing u'_∞/U_∞.

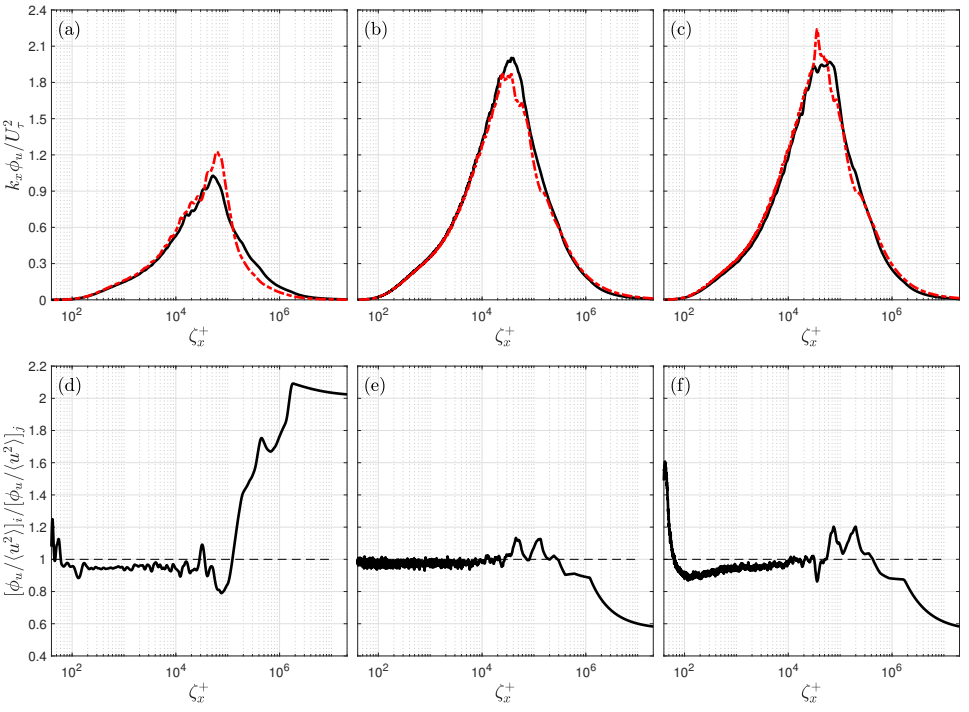

FIGURE 2. Pre-multiplied velocity spectra in the free-stream for cases (a) G and H, (b) K and M, and (c) N and O. (—) cases G, K, and N; (– · –) cases H, M, and O. The bottom panes (d), (e), and (f) show the ratio of the two curves presented in (a), (b) and (c), respectively; i represents the solid line and j represents the dashed line.

Before leaving this section, we draw the reader's attention to variation in $L_{u,\infty}$ for the various groups of cases in table 1. The variations in $L_{u,\infty}$ are a result of the changes to the active grid settings. For some groups, the variation in $L_{u,\infty}$ is marginal, however, we draw particular attention to cases G ($L_{u,\infty}/\delta = 2.5$) and H ($L_{u,\infty}/\delta = 1.7$) with a 50% change in integral scale at $u'_\infty/U_\infty \approx 8.1\%$, K ($L_{u,\infty}/\delta = 2.8$) and M ($L_{u,\infty}/\delta = 2.2$) with a 20% change in the integral scale at $u'_\infty/U_\infty = 12.0\%$, and N ($L_{u,\infty}/\delta = 1.6$) and O ($L_{u,\infty}/\delta = 2.7$) with a 65% change in the integral scale at $u'_\infty/U_\infty \approx 12.3\%$. We note that to achieve the same u'_∞/U_∞ for G and H, it was necessary to change U_∞ marginally, however, the ratio $U_\infty/U_\tau = U_\infty^+$ was approximately the same for both cases.

The free-stream spectra associated with the identified cases with significant differences in $L_{u,\infty}$ are shown in figure 2(a-c). The area under the two curves in each pair is approximately equal because u'/U_τ is approximately the same for each pair. While the spectra may appear quite similar at first, this is a consequence of the fact that a high $Re_{\lambda,\infty}$ turbulent field has a relatively fixed shape. The ratio of each set of curves is shown in figure 2(d-f), where the difference between the free-stream flows is more apparent; peaks on the order of 20% difference exist at the peak in the premultiplied spectrum, signifying a significant change in the energy distribution for the same $Re_{\lambda,\infty}$.

3. Impact on the boundary layer

Wall-normal profiles of the inner-normalised mean velocity and variance profiles are provided in figures 3(a) and (b), respectively. The eye is immediately drawn to the collapse of the flows at a given u'_∞/U_∞ for both the mean velocity and the variance.

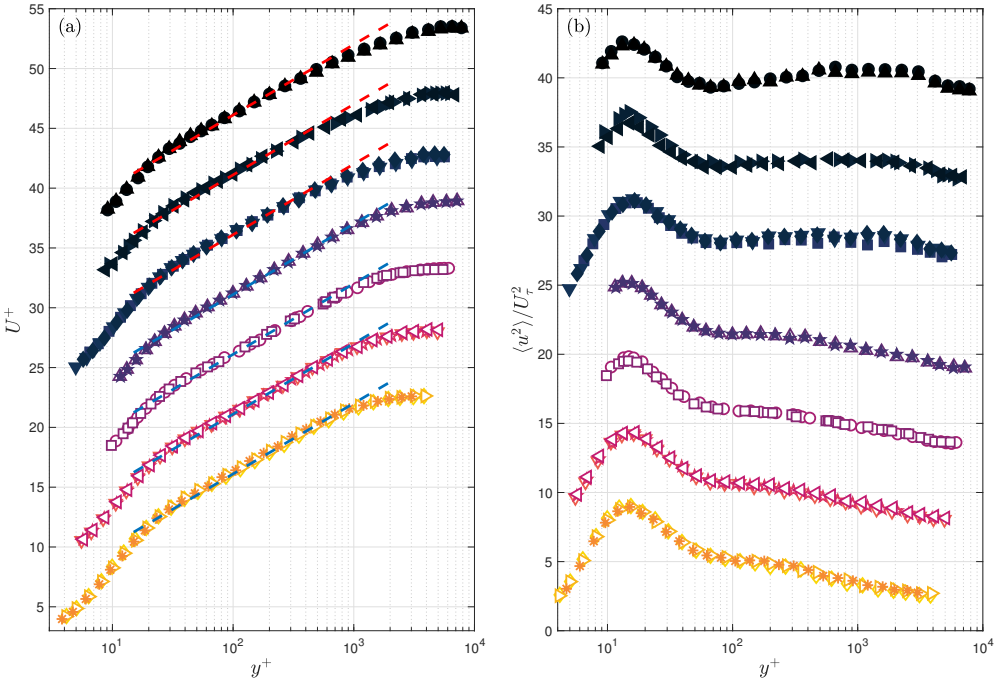

FIGURE 3. Wall-normal profiles of the (a) mean velocity and (b) turbulent fluctuations, both normalised by wall-units. See table 1 for symbols. Lightest to darkest symbols represent increasing u'_∞/U_∞. Each set of profiles have approximately the same u'_∞/U_∞ and are offset by +5 from one-another. In (a) the parameters used for the log-law fit are $\kappa = 0.39$ and $\mathcal{B} = 4.3$, which are taken roughly from Marusic *et al.* (2013).

The similarity between the curves in the log-law region can be quantified by κ in table 1, where the difference in κ between the cases with matched u'_∞/U_∞ does not exceed 0.03. Furthermore, for a given group of profiles, δ and $U_\infty/U_\tau = U_\infty^+$ do not change appreciably. This is particularly significant given that it also holds for the previously identified pairs where $L_{u,\infty}$ changes by up to 65% and U_∞ changes by 1 m/s (representing a 20% change in bulk energy). This suggests that the bulk characteristics of the TBL subjected to FST are dependent primarily on u'_∞/U_∞ and $Re_{\lambda,\infty}$ rather than $L_{u,\infty}$. This also suggests that figure 11(a) in Dogan *et al.* (2016) that shows the variance gain in the boundary layer for different u'_∞/U_∞ may be sufficient to predict the variance profile given the free-stream turbulence intensity.

Similar characteristics are present in the higher-order statistics for these flows. Namely, the velocity skewness ($S_u = \langle u^3 \rangle / \langle u^2 \rangle^{3/2}$) and flatness ($F_u = \langle u^4 \rangle / \langle u^2 \rangle^2$) are plotted for each case in figures 4(a) and (b), respectively, and demonstrate that for a given u'_∞/U_∞ these statistics are approximately collapsed near the wall. Some scatter is present in the free-stream, particularly visible in the flatness, however, nearer the wall all the curves are collapsed, suggesting the near-wall dynamics are the same. The values of S_u and F_u both resemble those measured previously by Sharp *et al.* (2009) in a similar set-up. Ultimately, the results demonstrate that at these $Re_{\lambda,\infty}$ the intermittent discontinuity between the canonical laminar free-stream and a turbulent boundary layer does not exist for these flows with FST, but rather the flow takes on the characteristics of approximately homogeneous, isotropic turbulence near the outer regions of the boundary layer. For reference, a Gaussian distribution has $S_u = 0$ and $F_u = 3$.

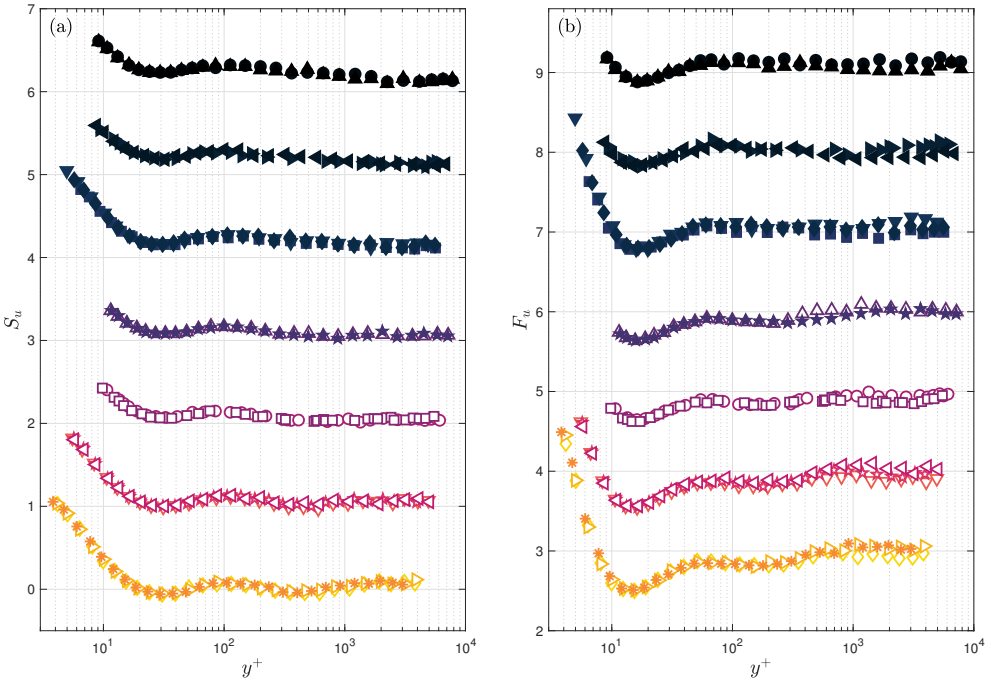

FIGURE 4. Wall-normal profiles of the streamwise velocity (a) skewness and (b) flatness. See table 1 for symbols. Lightest to darkest symbols represent increasing u'_∞/U_∞. Each set of profiles have approximately the same u'_∞/U_∞ and are offset by +1 from one-another.

Further insight on the resilience of the boundary layer to changes in the FST can be gained by looking at the spectral distribution of energy, viz. the spectrograms, which are shown in figure 5 for the cases with the identified significant changes in $L_{u,\infty}$. For brevity, we define $\phi^+ = k_x\phi_u/U_\tau^2$. All flows exhibit spectral inner and outer peaks, similar to observations made in canonical TBLs (Hutchins & Marusic 2007*a*). The inner peak is situated at a wavelength of $\zeta_x^+ \approx 1000$ and a wall-normal position of $y^+ \approx 15$, for all cases, in agreement with previous investigations in canonical TBLs (Hutchins & Marusic 2007*a*) and TBLs subjected to FST (Dogan *et al.* 2016, 2017). The outer peak is situated near $\zeta_x/\delta \approx 10$ and $y/\delta \approx 0.4$, which is substantially higher than where it is found in canonical TBLs at similar Re_τ (Hutchins & Marusic 2007*a*). This is because the outer peak is effectively imposed on the boundary layer by the free-stream spectrum. Further comparison of the present flows with canonical zero-pressure-gradient spectrograms is presented by Dogan *et al.* (2016).

Qualitatively, each pair of spectrograms look quite similar, and we thus present their differences in the right hand panes of figure 5. Despite the similar appearance of the spectrogram for each pair there are differences in the large scales present all the way to the wall. These differences are quantified by the parameter $\Delta^+ = (\phi_a^+ - \phi_b^+)/\phi_a^+$ (where a and b can be any pair of test cases from table 1), demonstrating differences between the flows on the order of 40% exist near the wall at large wavelengths. The strips of high-difference that track from the outer region all the way to the lowest measurement station are directly correlated to the differences in the free-stream spectra shown in figure 2(d-f), thus the differences in the free-stream spectra track all the way to the wall. In contrast, the spectra at low ζ_x are nearly identical for each pair. This is illustrated explicitly for the spectra at the near wall peak, $y^+ \approx 15$, in figure 6, where the small scales are

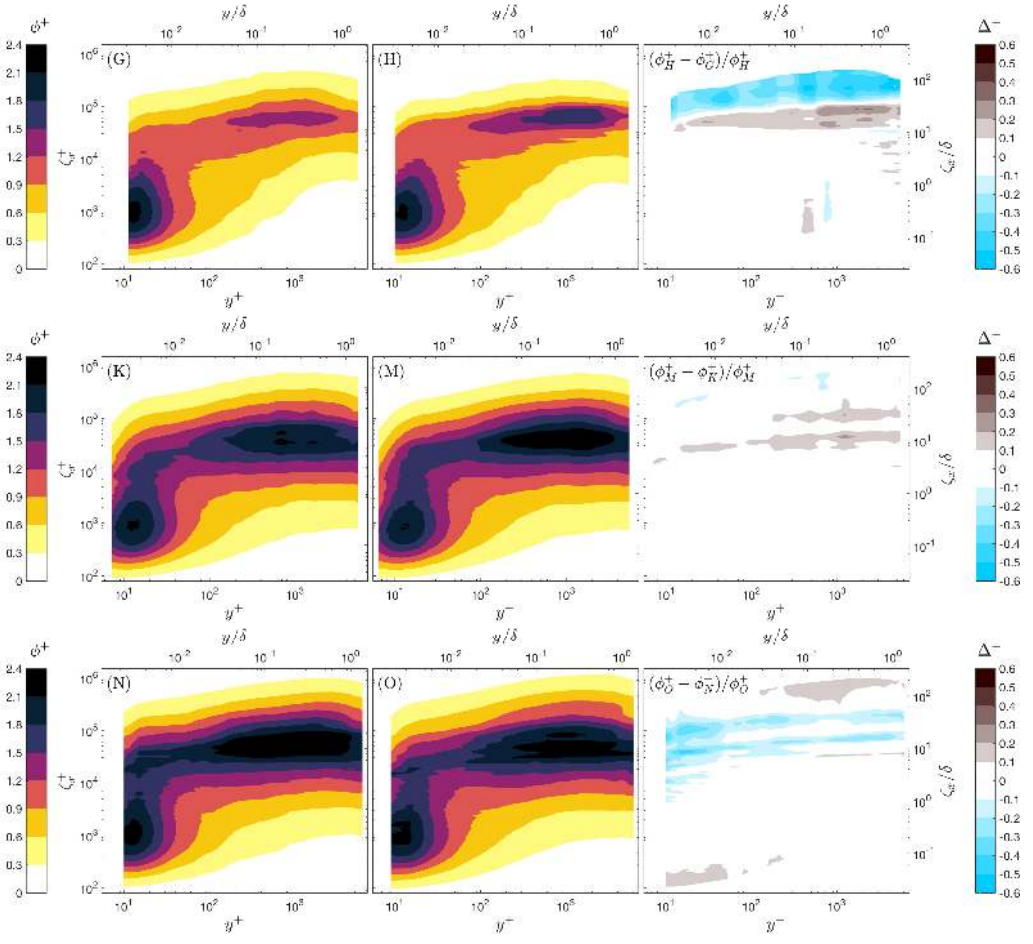

FIGURE 5. Spectrograms of the inner-normalised pre-multiplied velocity spectra for pairs of test cases with the same turbulence intensity but different integral scales. The illustrated test name is given in each pane of the figure. The differences between these spectrograms are shown in the right-hand panes of the figure as $\Delta^+ = (\phi_a^+ - \phi_b^+)/\phi_a^+$, where a and b can be any pair of test cases.

collapsed but there is still a difference in the large scales for all cases. Moreover, the least turbulent case (A) and the most turbulent case (Q), which differ in both U_∞ and u'_∞/U_∞ by a factor of 1.8 or greater, are contrasted in figure 7, showing that they differ nearly everywhere except the near-wall peak. Finally, the spectral coherence,

$$\gamma^2 = \frac{|\phi_{u(y_{\text{inner}})u(y_{\text{outer}})}|^2}{\phi_{uu(y_{\text{inner}})}\phi_{uu(y_{\text{outer}})}}, \tag{3.1}$$

between the inner peak location ($y^+_{\text{inner}} \approx 15$) and a location in the log-layer ($y^+_{\text{outer}} \approx 600$) is illustrated for cases G, H, and N in figure 8; these cases were used because they were acquired with the four-wire set-up of Dogan *et al.* (2017). The outer location was dictated by the fixed separation between the wires on the moving rake. The coherence was filtered with a 25% bandwidth moving filter as per Baars *et al.* (2016). The coherence figure illustrates that there is no correlation between wavelengths below $\zeta_x^+ = 7000$ for these three cases. This provides more evidence that the small scales are independent of the large scale organisation in the log-layer. We note that $\zeta_x^+ = 7000$ or similar values were found

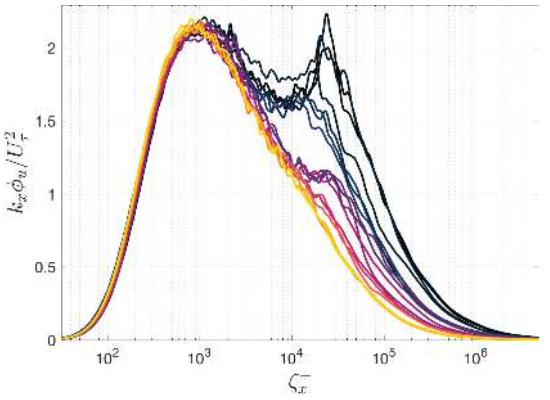

FIGURE 6. Inner-normalised pre-multiplied spectra for all cases in table 1 at $y^+ \approx 15$. Lines are coloured from lightest to darkest in order of increasing turbulence intensity.

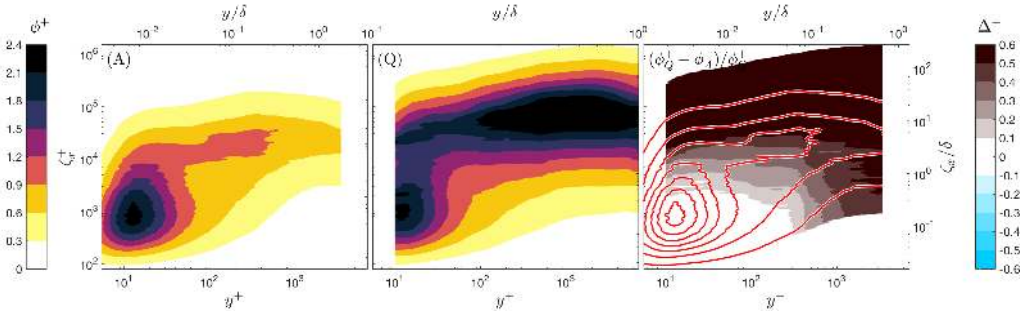

FIGURE 7. Spectrograms of the inner-normalised pre-multiplied velocity spectra for cases A and Q from table 1. The difference between these spectrograms are shown in the right-hand pane as $\Delta^+ = (\phi_Q^+ - \phi_A^+)/\phi_Q^+$. The contour lines in the right-hand pane identify the location of the inner peak for case A.

to approximately separate the inner and outer peaks independently of Re_τ in previous studies (Hutchins & Marusic 2007*b*; Mathis *et al.* 2009; Baars *et al.* 2016; Marusic *et al.* 2017). It is not immediately clear why this particular value should be meaningful, but it is reproducable for different Re_τ and u'_∞/U_∞ here, and is present in other studies. The overall picture painted by the above is that the spectral distribution of the FST leaves a footprint on the energy signature at the wall, but for a given u'_∞/U_∞ (within the tested range) does not influence the mean properties of the flow or the small-scales of the flow across the entire range of wall-normal locations.

An alternative way of looking at the spectrograms is to plot them as a 'gain' function relative to the spectrum in the free-stream. We define this gain function as the ratio between the local spectrum and the free-stream spectrum at each wavenumber and wall-normal position, $G(k_x, y) = \phi^+(k_x, y)/\phi_\infty^+(k_x)$. These gains are illustrated in figure 9 for the previously identified pairs. Additional contour lines are included at $\phi^+ = 0.6$ to identify the energetic region of the spectra. Like the spectrograms, the gain plots are remarkably similar, particularly within the region enclosed by the $\phi^+ = 0.6$ thresholds. The difference is quantified in the right-hand panes of figure 9 by the parameter $\Delta_G = (G_a - G_b)/G_a$ (where a and b are any two cases from table 1), which supports the notion that the gain plots are similar in the most relevant region.

The concept of the spectral gain function is particularly useful if there was a single

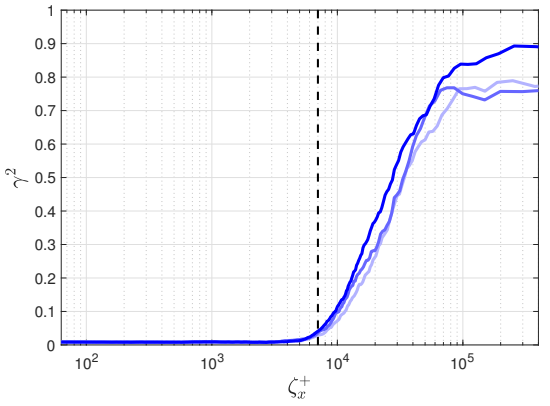

FIGURE 8. Spectral coherence between the inner peak ($y^+_{\text{inner}} = 15$) and a position in the log-layer for cases: G ($y^+_{\text{outer}} = 619$), H ($y^+_{\text{outer}} = 556$), and N ($y^+_{\text{outer}} = 630$). Lines from lightest to darkest are G, H, and N. The vertical dashed line is at $\zeta_x^+ = 7000$.

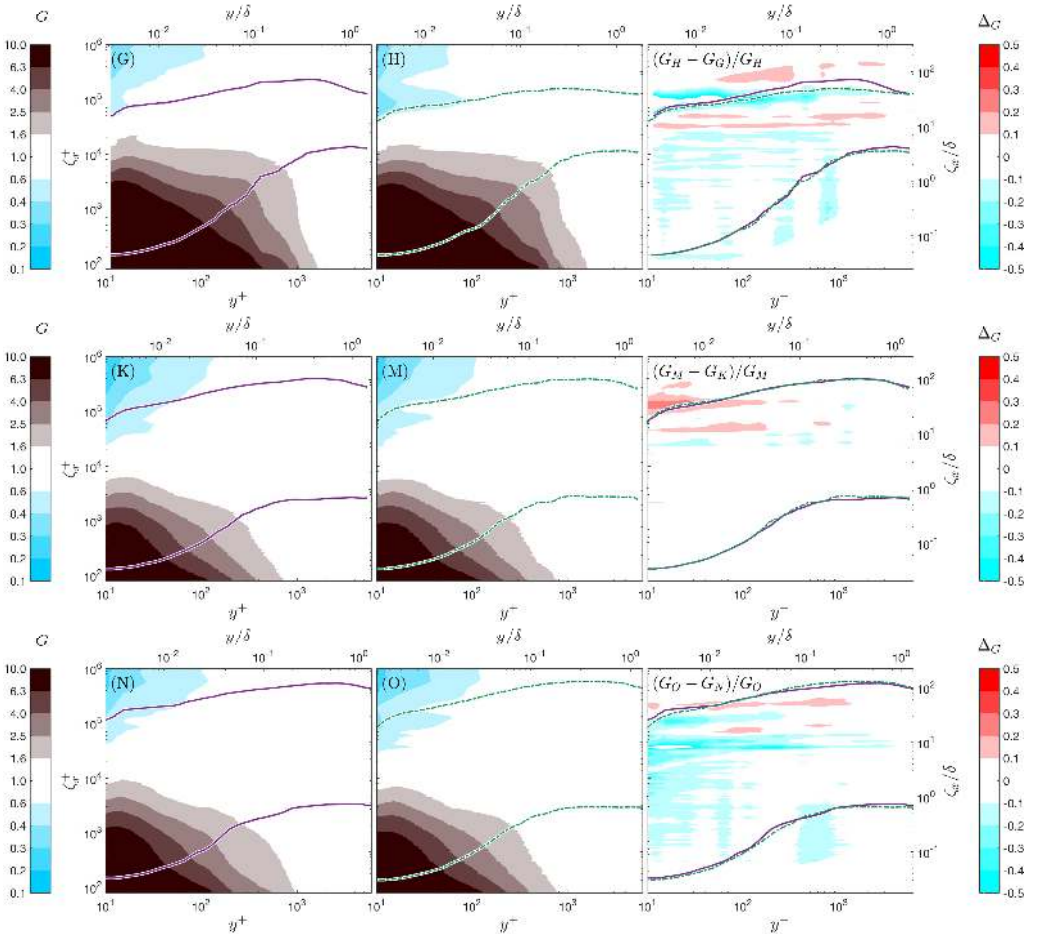

FIGURE 9. Contour plots of the gain of the pre-multiplied velocity spectra relative to the free-stream spectrum and the difference between the shown cases. Additional contour lines are drawn at a threshold of $\phi^+ = 0.6$ to identify the area in the plot that represents the most energy.

global gain function (G_g) that could be used to predict the spectrogram of a turbulent boundary layer given an arbitrary free-stream turbulence spectrum. This could then be integrated to give the variance profile. The above observations based on the spectrograms are insightful, but beg at least two questions. The first is whether the separation in $L_{u,\infty}/\delta$ between the cases is in fact sufficient to make meaningful observations. The second is whether such a global G_g function exists and can reproduce the boundary layer spectrogram from just the free-stream spectrum. These concerns are addressed in the next section.

4. Implications and discussion

Given the spectrograms and velocity profiles for each group of cases at matched u'_∞/U_∞ are so markedly similar, it is natural to wonder if the free-stream conditions were sufficiently different between cases to begin with. We first remind the reader that the intention of this study was to keep certain parameters constant (u'_∞/U_∞ and $Re_{\lambda,\infty}$) while varying others ($L_{u,\infty}$ and the overall large scale organisation). To this end, we must demonstrate that the varied conditions are sufficiently different from one another. First, the largest change in $L_{u,\infty}/\delta$ investigated here is from 1.6 for case N to 2.7 for case O. This is over an entire δ change. This change is also comparable to the relative change in $L_{u,\infty}$ produced by Shahinfar & Fransson (2011), who did observe a measurable impact on transition; in dimensional units, the change here is an order of magnitude larger than in Shahinfar & Fransson (2011). Moreover, this change in $L_{u,\infty}/\delta$ covers $\sim 25\%$ of the range of the experiments of Hancock & Bradshaw (1983), who did report an impact of $L_{u,\infty}$ on the TBL for lower values of u'_∞/U_∞; recall there is some ambiguity relating to the means by which they interpreted their integral scales. Second, for the comparison between G and H the mean velocity changes result in a significant difference in total energy in the mean flow, $(U^2_{\infty,G} - U^2_{\infty,H})/U^2_{\infty,G} \approx 0.2$, but the profiles and spectrograms remain the same. We also remind the reader that for a turbulent free-stream at a given $Re_{\lambda,\infty}$, the shape of the spectrum is relatively fixed and the only part of the spectrum that can be varied between cases is the largest scales (Hearst & Lavoie 2015), which are beyond the peak in the pre-multiplied spectrum. Finally, and perhaps most convincingly, in figure 5 the difference spectrograms show that the difference in the spectra in the free-stream between cases is felt all the way to the lowest measurement station at the large wavelengths. Nonetheless, the impact on the mean statistics is negligible (for a given u'_∞/U_∞). If there had been a factor of 10 change in $L_{u,\infty}$ while keeping u'_∞/U_∞ fixed (which we note is seemingly not possible with an active grid (Larssen & Devenport 2011; Hearst & Lavoie 2015) and in this facility would result in a length scale comparable to the size of the facility), pushing it to even larger wavelengths, the difference in the spectra would still exist all the way to the wall, but there is no reason to believe that those larger wavelengths would have a stronger presence. The alternative would be to make $L_{u,\infty}$ smaller, in order to inject energy at the same wavelength as the inner peak, however, this may not physically be possible (in the sense of fully-developed FST over a TBL because a turbulent spectrum at a given $Re_{\lambda,\infty}$ has a given shape that does not vary by much at the small scales).

The second item that deserves further discussion is the significance of a global gain function G_g. To test this concept, we produce a global gain function $G_g(k_x, y)$ that is simply the average of the gain functions from all but three cases in table 1; cases C, G, and N are reserved to test the methodology because they represent a distribution of the turbulence intensities realised in this experiment. We are happy to perform this average because the spectrograms (figure 5) and gain functions (figure 9) were remarkably

similar within the region that contained the most energy. We then reconstruct the spectrograms for our reserved cases (C, G, N) that were not included in the formation of G_g based on the global gain function, $\tilde{\phi}^+(k_x, y) = G_g(k_x, y) \cdot \phi^+_\infty$. The reconstructed spectrograms are given in figures 10(a), (b), and (c), respectively, with the differences between the reconstruction and the original spectrograms, $\Delta_C = (\phi^+ - \tilde{\phi}^+)/\phi^+$, given in figures 10(d), (e), and (f). To guide the eye and to facilitate comparison with the measured spectrograms, contours are drawn for every 0.3 increment in ϕ^+ starting from $\phi^+ = 0.9$. What is significant here is that a single G_g can approximately reconstruct the spectrogram for these test cases and identify the location of both the inner and outer peak. In particular, for these cases the outer peak is resolved to within 10% (for the worst case which is the lowest u'_∞/U_∞ case C), and the inner peak location appears accurate, but it's magnitude is resolved to within 40% (for the worst case which is the highest u'_∞/U_∞ case N). This identifies that the particular form of G_g found here is not 'universal', but it also provides a key point of insight. The ability of the approach to predict the position and magnitude of the outer peak to within 10% for these diverse cases suggests there is a consistent manner in which the boundary layer filters and selectively amplifies the spectra in the outer region of the TBL subjected to FST. Furthermore, the failure of the 'gain' methodology to capture the small wavelengths near the wall is because it is superseded by a different universality. That is, the spectrograms at small wavelengths near the wall are the same in viscous units, independent of both Re_τ and u'_∞/U_∞. This was illustrated at $y^+ \approx 15$ for all cases in figure 6 and by contrasting the most and least intense free-stream flows in figure 7. This echoes the observation by Dogan *et al.* (2016) that the spectral inner peak remains in the same location for increasing u'_∞/U_∞ and further identifies that its shape and magnitude are also independent of u'_∞/U_∞. The primary energetic region not captured by either the 'universal' near-wall peak or the outer region gain function is the large wavelengths close to the wall. While this region is similar for cases with fixed u'_∞/U_∞ (figure 6), it becomes more energetic with increasing u'_∞/U_∞, which in turn results in higher Re_τ.

In figure 10 the wall-normal position $y^+ = \sqrt{Re_\tau}$ is identified with a vertical dashed line. This location appears to consistently separate the near-wall flow (and the inner spectral peak) from the outer flow (and the outer spectral peak). It also roughly separates the region governed by the gain function and the region governed by the universal inner spectral peak. This is consistent with the mean momentum balance physical model of the boundary layer (Klewicki *et al.* 2007, 2009) and represents the approximate extent to which viscous forces play a dominant role. This $\sqrt{Re_\tau}$ scaling is also thought to hold for the smallest wall-attached eddies (Klewicki *et al.* 2009; Marusic *et al.* 2013) and hence the beginning of the log-layer (Klewicki 2010). Marusic *et al.* (2017) showed that their outer scaling roughly held down to a lower limit of $y^+ \sim \sqrt{Re_\tau}$. Therefore, any scale with sufficient energy that is larger than this smallest attached-eddy will likely penetrate farther down to the wall. The figures suggest that the smaller-scale FST fluctuations appear to be attenuated. In fact, all fluctuations are attenuated and only the large-scales in the FST are able to penetrate through to the wall as they contain significantly more energy than the wall-attached eddy at every wall-normal location.

From here, one can construct a conceptual model that appears to govern the spectral scaling for a TBL subjected to FST. For this model, the spectrogram is divided into four regions separated along $y^+ = \sqrt{Re_\tau}$ and $\zeta^+_x = 7000$. The divider in wavelength separates the large and small scales as discussed in the previous section. These regions are depicted in figure 11(b) and can be described as follows:

I. $(y^+ < \sqrt{Re_\tau}, \zeta^+_x < 7000)$: This region is home to the near-wall spectral peak (typically centred at $y^+ \approx 15$, $\zeta^+ \approx 1000$). The near-wall spectral peak scales with

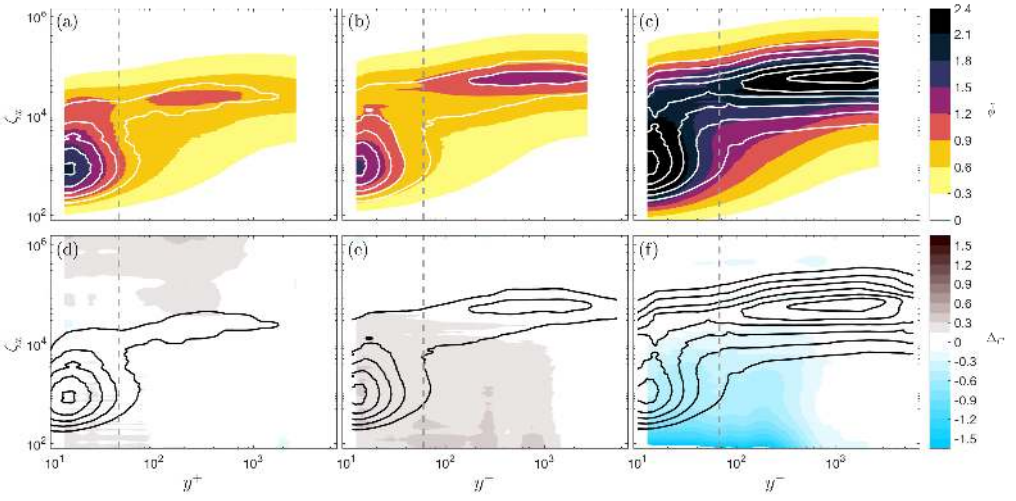

FIGURE 10. Reconstructed spectrograms based on the global gain map for (a) case C, (b) case G, and (c) case N from table 1. The corresponding difference maps between the reconstructed and measured spectrograms are given in (d), (e), and (f), respectively, as $\Delta_C = (\phi^+ - \tilde{\phi}^+)/\phi^+$. The solid lines represent contours at $\phi^+ = 0.9$, 1.2, 1.5, 1.8 and 2.1 from the measured spectrograms. The solid line contours increase from outer most to inner most. The vertical dashed lines are at $y^+ = \sqrt{Re_\tau}$.

viscous units, making its location, shape, and normalised magnitude universal. This means that we can use this information to obtain skin-friction of boundary layers under the influence of FST. For example, a hot-wire measurement in the near-wall region could be used in liaison with scaling identified here to determine U_τ and hence C_f by adjusting the estimate of U_τ until the inner peak was collapsed on the expected value.

II. ($y^+ < \sqrt{Re_\tau}, \zeta_x^+ > 7000$): This region is influenced by variations in the FST. Increases in u'_∞/U_∞ penetrate all the way to the wall, resulting in an increase in U_τ and correspondingly Re_τ. This occurs because the energy that exists at the large wavelengths is not transferred to the near-wall peak in region (I) such that the latter is fixed and universal. Note that because the near-wall peak in region (I) is collapsed for all tested u'_∞/U_∞ and Re_τ, it suggests that the increase in area under the spectral curve at $\zeta_x^+ > 7000$ is proportional to the growth in U_τ. Changes in $L_{u,\infty}$ penetrate down to this region (figure 5), but do not appear to influence the mean velocity or variance profiles for the u'_∞/U_∞ investigated here.

III. ($y^+ > \sqrt{Re_\tau}, \zeta_x^+ > 7000$): In this region, the boundary layer acts as a universal filter to the most energetic wavelengths in the free-stream spectrum. It preferentially amplifies certain wavelengths, resulting in the outer peak. The amplification is independent of u'_∞/U_∞, and hence this region is governed by global laws different from those in region (I).

IV. ($y^+ > \sqrt{Re_\tau}, \zeta_x^+ < 7000$): This region is not home to a significant amount of the energy and seemingly does not play as strong a role in the dynamics.

This model explains the increase in U_τ with increasing u'_∞/U_∞ and suggests that a measurement at $y^+ \approx 15$ is sufficient to estimate U_τ for these flows. Futhermore, one can in principle predict the location of both the inner and outer spectral peaks given the spectrum of the FST. This is because G_g approximately describes the flow in regions (II), (III) and (IV), and region (I) is independent of the other regions. We thus propose

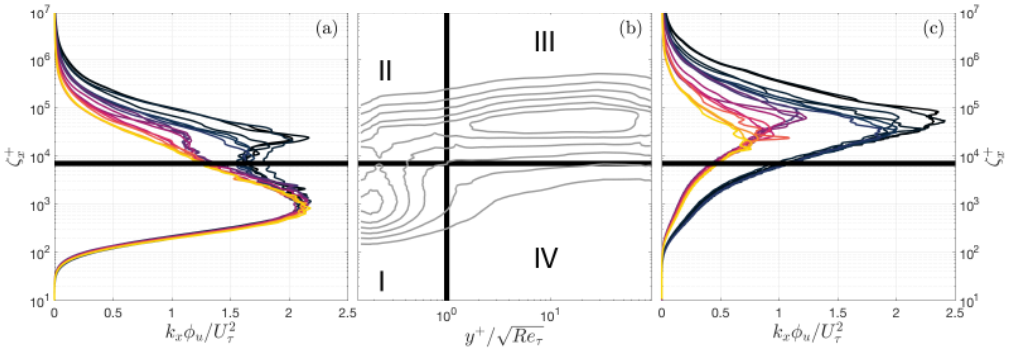

FIGURE 11. (a) Inner-normalised pre-multiplied spectra at $y^+ \approx 15$ for all cases. (b) Conceptual map identifying four regions in a generic spectrogram of a TBL subjected to FST. (c) Inner-normalised pre-multiplied spectra in the free-stream for all cases. For the spectra, the lightest to darkest lines represent increasing u'_∞/U_∞. The identified regions are separated along $y^+/\sqrt{Re_\tau} = 1$ and $\zeta^+ = 7000$.

using G_g to reconstruct the flow in regions (II), (III), and (IV) from only the free-stream spectrum, and then using the inner peak from our best resolved case (A) in region (I) to reconstruct the same cases as shown in figure 10. Ideally, the inner peak geometry would come from an analytical expression, however, for the time being our best resolved measurement of the empirical curve will suffice. This proposed reconstruction process is illustrated in figure 12, where weighting functions are used to blend the inner peak reconstruction (region (I)) with the gain reconstruction (regions (II)-(IV)). The weighting decays linearly outside of the bounds specified in the conceptual model to a total extent of 5 times the limit. The results of this reconstruction are presented in figure 13, where it can be seen that both the inner and outer peaks are now captured by the reconstruction methodology based on only the free-stream spectrum; both the location and magnitude of the inner peak are now in agreement between the reconstruction and the measured spectrograms to within 6%, a vast improvement over figure 10 where only the gain function was used.

5. Conclusions

The influence of the large-scale organisation of an external turbulent flow on a turbulent boundary layer was investigated experimentally by generating free-stream turbulence flows where the turbulence intensity (u'_∞/U_∞) and Reynolds number ($Re_{\lambda,\infty}$) were fixed, but the free-stream integral scale ($L_{u,\infty}$) and the distribution of energy in the spectrum was varied. This was achieved by generating free-stream turbulence with an active grid over a false floor in a wind tunnel. While a wide array of tests were presented, three specific groupings with (i) $u'_\infty/U_\infty = 8.2\%$; $Re_{\lambda,\infty} \approx 455$, (ii) $u'_\infty/U_\infty = 12.0\%$; $Re_{\lambda,\infty} \approx 525$, and (iii) $u'_\infty/U_\infty = 12.3\%$; $Re_{\lambda,\infty} \approx 615$, were investigated with integral scales changing between 20% and 65%. It was found that the longitudinal mean velocity, variance, skewness, and flatness profiles, as well as the peaks in the spectrograms appear to be approximately collapsed for a given turbulence intensity, and are thus dependent only on u'_∞/U_∞ and $Re_{\lambda,\infty}$ for the cases investigated here. This result appears to contrast with earlier results, e.g., Hancock & Bradshaw (1983, 1989), which were conducted at much lower $Re_{\lambda,\infty}$ and u'_∞/U_∞, and where the estimation of the integral scale may have been susceptible to errors associated with the equation used. Regardless, for a range of $L_{u,\infty}/\delta$ that overlapped with the region where previous studies showed an impact of

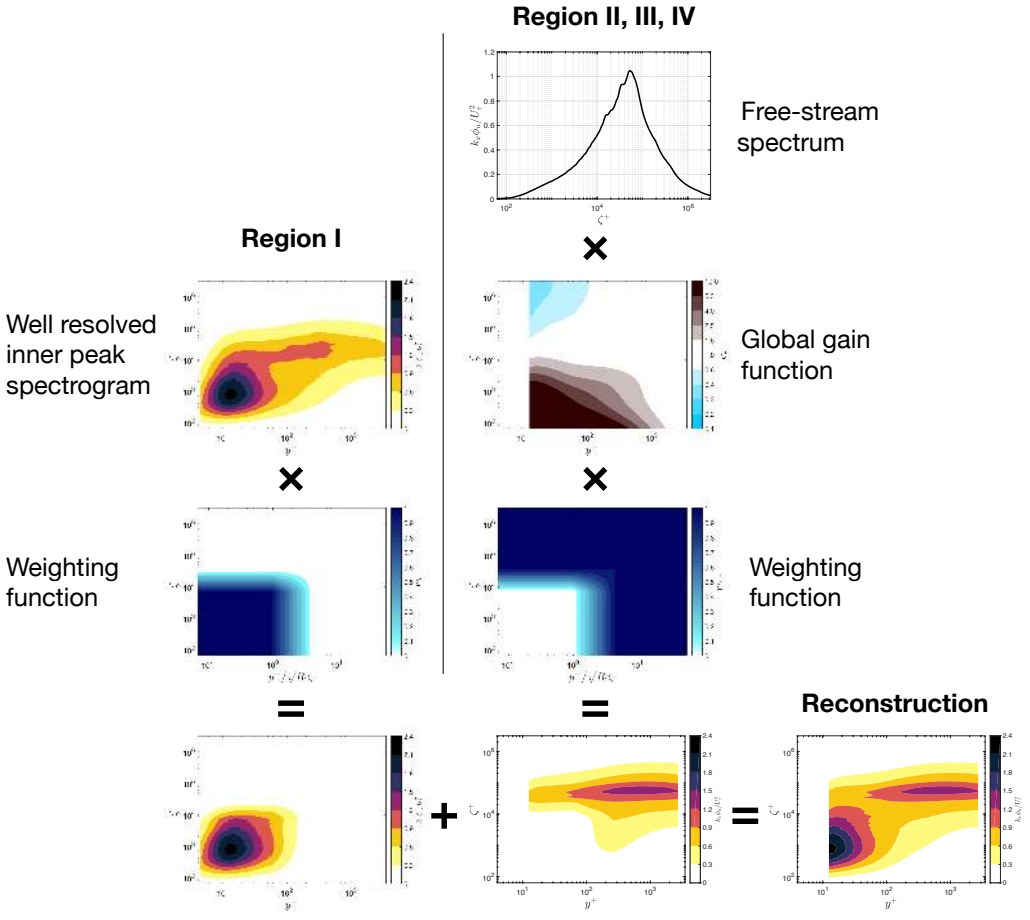

FIGURE 12. Proposed reconstruction methodology. Region (I) in figure 11 is constructed from the inner peak of a well-resolved case. Regions (II), (III) and (IV) are constructed by multiplying the free-stream spectrum by the global gain function (G_g) and a weighting function. These two spectrograms are then summed to produce the reconstruction.

$L_{u,\infty}$, none was observed here. If this was not an err in the previous campaigns, it may be a result of the increased $Re_{\lambda,\infty}$ here. It was explicitly demonstrated that the large scales of the spectrograms remain disparate between cases with matched u'_∞/U_∞ right to the wall if they have different $L_{u,\infty}$. Nonetheless, this does not result in changes to the mean statistics.

It was also demonstrated that a gain function could be composed that approximately reproduced the outer peak in the spectrograms of the TBL subjected to FST using only the spectrum in the free-stream. This same function was able to estimate the location of the near-wall peak as well, but the magnitude was only within 40% of the measured magnitude. This failure was a result of the seemingly universal nature of the near-wall peak, which was shown to have the same location and magnitude (in inner units) independent of the FST. A conceptual model was suggested, identifying that the outer boundary layer filters the free-stream spectrum using a global gain function, and then always produces the same universal near-wall peak. Because the excess energy that penetrates down through the boundary layer for an increase in u'_∞/U_∞ cannot be transferred to the universal near-wall peak, it must remain at larger wavelengths and

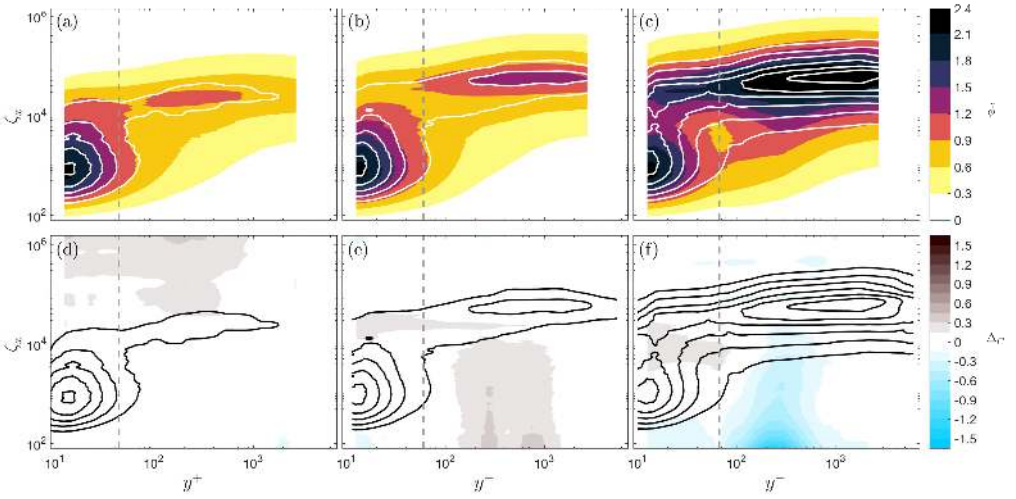

FIGURE 13. Reconstructed spectrograms using the methodology presented in figure 12 for (a) case C, (b) case G, and (c) case N from table 1. The corresponding difference maps between the reconstructed and measured spectrograms are given in (d), (e), and (f), respectively, as $\Delta_C = (\phi^+ - \tilde{\phi}^+)/\phi^+$. The solid lines represent contours at $\phi^+ = 0.9$, 1.2, 1.5, 1.8 and 2.1 from the measured spectrograms. The solid line contours increase from outer most to inner most. The vertical dashed lines are at $y^+ = \sqrt{Re_\tau}$.

results in an increase in U_τ. This model allows for the description of the spectrograms of a TBL subjected to FST *a priori*, with only knowledge of the free-stream spectrum, and describes the mechanism for the increase in U_τ with increasing u'_∞/U_∞. It was also able to demonstrably reconstruct the boundary layer spectrogram, resolving both the inner and outer peaks within 10%, given only the free-stream spectrum, U_τ and δ.

The authors acknowledge the financial support of the European Research Council (ERC Grant agreement No. 277472), and the Engineering and Physical Sciences Research Council of the United Kingdom (EPSRC Grant Ref. No. EP/L006383/1). RJH was partially funded by the Natural Sciences and Engineering Research Council of Canada (NSERC) while at the University of Southampton. ED was partially funded by Zonta International while at the University of Southampton.

REFERENCES

BAARS, W. J., HUTCHINS, N. & MARUSIC, I. 2016 Spectral stochastic estimation of high-Reynolds-number wall-bounded turbulence for a refined inner-outer interaction model. *Phys. Rev. F* **1** (054406).

BRANDT, L., SCHLATTER, P. & HENNINGSON, D. S. 2004 Transition in boundary layers subject to free-stream turbulence. *J. Fluid Mech.* **517**, 167–198.

CASTRO, I.P. 1984 Effects of free stream turbulence on low Reynolds number boundary layers. *J. Fluids Eng.* **106** (3), 298–306.

CORRSIN, S. 1963 Turbulence: experimental methods. In *Handbuch der Physik* (ed. S. Flügge & C.A. Truesdell), pp. 524–589. Springer.

DOGAN, E., HANSON, R. & GANAPATHISUBRAMANI, B. 2016 Interactions of large-scale free-stream turbulence with turbulent boundary layers. *J. Fluid Mech.* **802**, 79–107.

DOGAN, E., HEARST, R. J. & GANAPATHISUBRAMANI, B. 2017 Modelling high Reynolds number wall-turbulence interactions in laboratory experiments using large-scale free-stream turbulence. *Phil. Trans. R. Soc. A* **375** (2089), 20160091.

Ertunç, Ö., Özyilmaz, N., Lienhart, H., Durst, F. & Beronov, K. 2010 Homogeneity of turbulence generated by static-grid structures. *J. Fluid Mech.* **654**, 473–500.

Esteban, L. B., Dogan, E., Rodríguez-López, E. & Ganapathisubramani, B. 2017 Skin-friction measurements in a turbulent boundary layer under the influence of free-stream turbulence. *Exp. Fluids* **58** (9), 115.

Fransson, J. H. M., Matsubara, M. & Alfredsson, P. H. 2005 Transition induced by free-stream turbulence. *J. Fluid Mech.* **527**, 1–25.

Hack, M. J. P. & Zaki, T. A. 2014 Streak instabilities in boundary layers beneath free-stream turbulence. *J. Fluid Mech.* **741**, 280–315.

Hancock, P. E. & Bradshaw, P. 1983 The effect of free-stream turbulence on turbulent boundary layers. *J. Fluids Eng.* **105**, 284–289.

Hancock, P. E. & Bradshaw, P. 1989 Turbulence structure of a boundary layer beneath a turbulent free stream. *J. Fluid Mech.* **205**, 45–76.

Hearst, R. J., Buxton, O. R. H., Ganapathisubramani, B. & Lavoie, P. 2012 Experimental estimation of fluctuating velocity and scalar gradients in turbulence. *Exp. Fluids* **53** (4), 925–942.

Hearst, R. J., Gomit, G. & Ganapathisubramani, B. 2016 Effect of turbulence on the wake of a wall-mounted cube. *J. Fluid Mech.* **804**, 513–530.

Hearst, R. J. & Lavoie, P. 2014 Decay of turbulence generated by a square-fractal-element grid. *J. Fluid Mech.* **741**, 567–584.

Hearst, R. J. & Lavoie, P. 2015 The effect of active grid initial conditions on high Reynolds number turbulence. *Exp. Fluids* **56** (10), 185.

Hearst, R. J. & Lavoie, P. 2016 Effects of multi-scale and regular grid geometries on decaying turbulence. *J. Fluid Mech.* **803**, 528–555.

Hutchins, N. & Marusic, I. 2007*a* Evidence of very long meandering features in the logarithmic region of turbulent boundary layers. *J. Fluid Mech.* **579**, 1–28.

Hutchins, N. & Marusic, I. 2007*b* Large-scale influences in near-wall turbulence. *Phil. Trans. R. Soc. A* **365**, 657–664.

Isaza, J. C., Salazar, R. & Warhaft, Z. 2014 On grid-generated turbulence in the near- and far field regions. *J. Fluid Mech.* **753**, 402–426.

Kang, H.S., Chester, S. & Meneveau, C. 2003 Decaying turbulence in an active-grid-generated flow and comparisons with large-eddy simulation. *J. Fluid Mech.* **480**, 129–160.

Klewicki, J., Fife, P. & Wei, T. 2009 On the logarithmic mean profile. *J. Fluid Mech.* **638**, 73–93.

Klewicki, J., Fife, P., Wei, T. & McMurtry, P. 2007 A physical model of the turbulent boundary layer consonant with mean momentum balance structure. *Phil. Trans. R. Soc. A* **365**, 823–839.

Klewicki, J. C. 2010 Reynolds number dependence, scaling, and dynamics of turbulent boundary layers. *J. Fluids Eng.* **132** (094001).

Kreilos, T., Khapko, T., Schlatter, P., Duguet, Y., Henningson, D. S. & Eckhardt, B. 2016 Bypass transition and spot nucleation in boundary layers. *Phys. Rev. F* **1** (043602).

Larssen, J. V. & Devenport, W. J. 2011 On the generation of large-scale homogeneous turbulence. *Exp. Fluids* **50**, 1207–1223.

Makita, H. 1991 Realization of a large-scale turbulence field in a small wind tunnel. *Fluid Dyn. Res.* **8**, 53–64.

Marusic, I., Baars, W. J. & Hutchins, N. 2017 Scaling of the streamwise turbulence intensity in the context of inner-outer interactions in wall turbulence. *Phys. Rev. F* **2** (100502).

Marusic, I., Monty, J. P., Hultmark, M. & Smits, A. J. 2013 On the logarithmic region in wall turbulence. *J. Fluid Mech.* **716** (R3).

Mathis, R., Hutchins, N. & Marusic, I. 2009 Large-scale amplitude modulation of the small-scale structures in turbulent boundary layers. *J. Fluid Mech.* **628**, 311–337.

Mydlarski, L. & Warhaft, Z. 1996 On the onset of high-Reynolds-number grid-generated wind tunnel turbulence. *J. Fluid Mech.* **320**, 331–368.

Nickels, T. B., Marusic, I., Hafez, S. & Chong, M. S. 2005 Evidence of the k_1^{-1} law in a high-Reynolds-number turbulent boundary layer. *Phys. Rev. Lett.* **95** (074501).

Nickels, T. B., Marusic, I., Hafez, S., Hutchins, N. & Chong, M. S. 2007 Some

predictions of the attached eddy model for a high Reynolds number boundary layer. *Phil. Trans. R. Soc. A* **365**, 807–822.

Rodríguez-López, E., Bruce, P. J. K. & Buxton, O. R. H. 2015 A robust post-processing method to determine skin friction in turbulent boundary layers from the velocity profile. *Exp. Fluids* **56** (4), 68.

Schlatter, P. & Örlü, R. 2012 Turbulent boundary layers at moderate Reynolds numbers: inflow length and tripping effects. *J. Fluid Mech.* **710**, 5–34.

Shahinfar, S. & Fransson, J. H. M. 2011 Effect of free-stream turbulence characteristics on boundary layer transition. *J. Phys: Conf. Ser.* **318** (032019).

Sharp, N., Neuscamman, S. & Warhaft, Z. 2009 Effects of large-scale free stream turbulence on a turbulent boundary layer. *Phys. Fluids* **21** (095105).

Smits, A. J., Monty, J. P., Hultmark, M., Bailey, S. C. C., Hutchins, N. & Marusic, I. 2011 Spatial resolution correction for wall-bounded turbulence measurements. *J. Fluid Mech.* **676**, 41–53.

Thormann, A. & Meneveau, C. 2014 Decay of homogeneous, nearly isotropic turbulence behind active fractal grids. *Phys. Fluids* **26** (025112).

Valente, P. C. & Vassilicos, J. C. 2012 Universal dissipation scaling for nonequilibrium turbulence. *Phys. Rev. Lett.* **108** (214503).

Vassilicos, J. C. 2015 Dissipation in turbulent flows. *Annu. Rev. Fluid Mech.* **47**, 95–114.

Vincenti, P., Klewicki, J., Morrill-Winter, C., White, C. M. & Wosnik, M. 2013 Streamwise velocity statistics in turbulent boundary layers that spatially develop to high Reynolds number. *Exp. Fluids* **54** (1629).

Wu, X., Moin, P., Wallace, J. M., Skarda, J., Lozano-Durán, A. & Hickey, J.-P. 2017 Transitional-turbulent spots and turbulent-turbulent spots in boundary layers. *Proc. Natl. Acad. Sci. U.S.A.* **114** (27), E5292–E5299.